RSC Advances

PAPER

View Article Online
View Journal | View Issue

Cite this: *RSC Adv.*, 2022, **12**, 297

One-step fabrication of soft calcium superhydrophobic surfaces by a simple electrodeposition process

Zhi Chen, *[a] Yongbo Hu,[a] Xu He,[a] Yihao Xu,[a] Xuesong Liu,[a] Yizhou Zhou,[a] Limei Hao[b] and Ying Ruan[a]

A simple, one-step electrodeposition process was rapidly performed on a metal substrate to fabricate calcium superhydrophobic surfaces in an electrolyte containing calcium chloride ($CaCl_2$), myristic acid ($CH_3(CH_2)_{12}COOH$), and ethanol, which can avoid the intricate post-processing of surface treatment. The morphology and surface chemical compositions of the fabricated superhydrophobic surfaces were systematically examined by means of SEM, XRD, and FTIR, respectively. The results indicate that the deposited surfaces were mainly composed of calcium myristate, which can dramatically lower surface free energy. The shortest process for constructing a superhydrophobic surface is about 0.5 min, and the maximum contact angle of the as-prepared surfaces can reach as high as 166°, showing excellent superhydrophobicity. By adjusting the electrodeposition time, the structure of the cathodic surface transforms from the turfgrass structure, loose flower structures, larger and dense flower structures, secondary flower structures, and then into tertiary or more flower structures. The superhydrophobic surfaces showed excellent rebound performance with a high-speed camera. After a pressing force, their hardness increases, but the superhydrophobic performance is not weakened. Inversely, the bouncing performance is enhanced. This electrodeposition process offers a promising approach for large areas of superhydrophobic surfaces on conductive metals and strongly impacts the dynamics of water droplets.

Received 9th August 2021
Accepted 24th November 2021

DOI: 10.1039/d1ra06019h

rsc.li/rsc-advances

1. Introduction

Wettability is one of the most significant and fundamental characteristics of solid materials, and it depends on the surface chemistry and morphology. The chemical compositions of the surface determine the surface energy, which has a significant effect on its wettability.[1–4]

There are many superhydrophobic surfaces in nature, such as rice leaves, rose petals, waterfowl feathers, strider legs, spider silk, and especially the famous lotus leaves.[5–7] Superhydrophobic surfaces have attracted wide attention because of their importance in scientific research and engineering. Two main factors are widely accepted common features of such surfaces: micro/nano rough structures and low surface free energy. Various methods and technologies have been employed successfully to prepare artificial superhydrophobic surfaces by controlling these two parameters. Several review articles have been published about different aspects of superhydrophobic surfaces.[8–11] However, most published methods suffer from many constraints such as specialized equipment, harsh conditions, multi-step procedures, and being very expensive and difficult to scale up for large areas in the fabrication process.[12] Recently, a few electrodeposition methods[13] have been widely used to prepare superhydrophobic surfaces on the electrode substrate due to their simplicity in adjusting the deposition parameters, low cost, and ease of scalability, especially applied on a wide range of materials. In 2012, Chen *et al.* reported[14,15] a new facile method for the electrodeposition of superhydrophobic surfaces. As a standard method, significant progress has been made over several years, including the use of Fe, Co, Ni, Cu, La, *etc.*, to prepare superhydrophobic surfaces.[16–19]

In addition, hydrogen has attracted extensive research interest owing to its environmental friendliness and high energy density. Recently, hydrogen bubbles arising from the electrochemical reduction of H^+ in the deposition process functioned as the soft template for electrodeposition products.[20–22] Hydrogen bubble templates have advantages compared with hard templates, including low cost, ease of preparation, and facile control and synthesis process. This method was gradually used to prepare superhydrophobic structures.[23] Meantime, calcium, the third most abundant metal in nature, had a decisive advantage over the other metals

[a]*School of Physical Science and Technology, Northwestern Polytechnical University, Xi'an 710129, China. E-mail: c2002z@nwpu.edu.cn; Fax: +86-29-88431664; Tel: +86-29-88431664*

[b]*Department of Applied Physics, School of Science, Xi'an University of Science & Technology, Xi'an, 710054, China*

due to its peculiar coordination chemistry. Although certain research about superhydrophobic surfaces, including calcium elements, has been reported in the literature,[24–26] to our knowledge, few studies have systemically reported about calcium superhydrophobic surfaces including preparation and certain impacting dynamic behaviors of water droplets, and their underlying mechanism is still not entirely clear.

In this work, a simple and effective method of the electrodeposition process offers promising approaches for large areas of superhydrophobic surfaces on conductive metals. The calcium superhydrophobic surface with the presence of a flower-like rough structure contributes to excellent bounce performance for water droplets. This study aims to reveal the influence of deposition time on surface morphology as well as wettability and bounce. Both the surface morphology and chemical compositions were carefully analyzed to reveal the formation mechanism of the electrodeposited superhydrophobic surface. The research on the impact of substrate hardness and type on bounce performance was reported systematically. Three metal materials, copper, aluminum, and stainless steel, differing in hardness, were compared to test the impacting velocity of different droplets and the substrate surface—the bounce behavior of water droplets under the influence of electrodeposition time, voltage, and external force. The analysis shows that the as-prepared surfaces are soft superhydrophobic surfaces and become harder after pressing by an external force. While the superhydrophobic surface does not lose its superhydrophobicity, its bounce performance has been enhanced. This method of electrodeposition is straightforward, effective, and low cost, which offers a promising approach for large areas of soft superhydrophobic surfaces on various conductive substrates.

2. Experimental section

2.1 Sample preparation

All the reagents and solvents were of analytical grade and used as received without any additional purification before use.[15,16] Before electrodeposition, two copper (or aluminum, or stainless steel) plates with a size of 50 mm × 25 mm × 1.5 mm were abraded with silicon carbide paper (400 and 800 grades), washed with distilled water multiple times, and then dried with a hair dryer.

In order to synthesize the superhydrophobic surfaces, the reference preparing conditions were 0.2 M calcium chloride and 0.1 M myristic acid in 150 ml ethanol electrolyte solution and the working distance between the cathode and anode in an electrolyte cell was kept at 30 mm, and a direct current (DC) voltage of 30 V was applied. To study the effects of preparing conditions on electrodeposited micro/nano structures, only one preparing condition was changed, and the others were fixed. The resulting samples were thoroughly rinsed with distilled water and ethanol. Finally, the obtained cathodic surfaces were dried in air for half an hour at room temperature. Subsequently, the as-prepared cathodic surface was prepared. Moreover, samples with various deposition times, voltages, and concentrations of calcium chloride were prepared.

2.2 Sample characterization

The obtained samples were characterized by field-emission scanning electron microscopy (FE-SEM, JSM-IT500). The infrared transmission spectra were recorded at room temperature on a BRUKER-Tensor27 Fourier-transform infrared spectrophotometer. X-ray diffraction (XRD) patterns were obtained using an X-ray diffractometer (Rigaku D/max-2550/PC). The

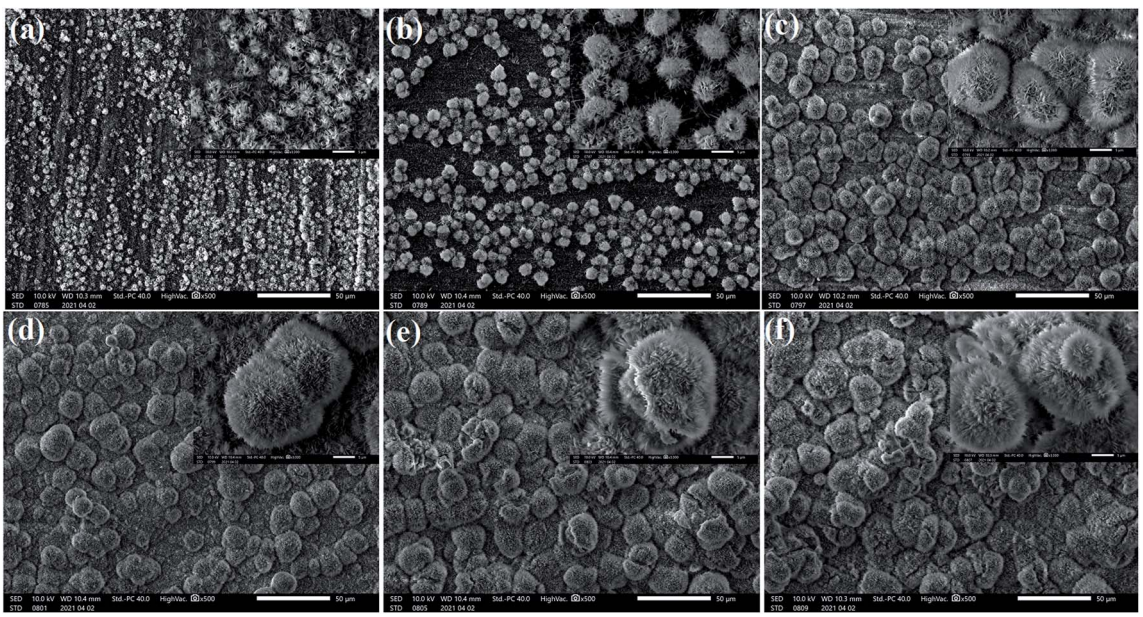

Fig. 1 SEM images of the cathodic copper surface in 0.1 M myristic acid and 0.2 M calcium chloride solution with a DC voltage of 30 V for different electrodeposition times: (a) 0.5 min; (b) 1 min 35 s; (c) 10 min; (d) 15 min; (e) 30 min; (f) 45 min.

contact angles were determined with a CCD (CNB-GP300 CGG1). The image data were recorded with a high speed camera (2000 fps, Revealer, 5F01-M). In addition, by setting the high-speed camera to 2000 frames per second, we have studied the bounce performance of water droplets' impact onto superhydrophobic surfaces.

3. Results and discussion

3.1 Morphology, wettability and chemical compositions of the copper superhydrophobic surfaces

The SEM measurement was used to characterize the morphology of the studied calcium surfaces, and the results are shown in Fig. 1. SEM images of the cathodic copper surface formed in the solution of 0.1 M myristic acid and 0.2 M calcium chloride at a varying time, namely, 0.5 min, 1 min 35 s, 10 min, 15 min, 30 min, and 45 min, are illustrated in Fig. 1(a)–(f). The representative images are from different samples produced under the same conditions except for the deposition times. As shown, with the electrodeposition in the solution for a short time (Fig. 1(a), 0.5 min), there appear a few random small crystallite clusters on the surface, and each cluster is like a loose bud with about a diameter of 2 μm (see the inset of Fig. 1(a)), and there are many microstructures similar to turfgrass. Prolonging the electrodeposition time to 1 min 35 s, the number of clusters increases and improves the uniformity of surfaces. As shown by the inset of Fig. 1(b), the high magnification image revealed that the cluster with a size of about 4 μm is formed, and each cluster is similar to that of 0.5 min. However, the difference is larger and denser. As the electrodeposition time is further extended to 10 min, the entire substrate is almost covered by the dense and homogeneous crystallite clusters. Each cluster has a size of about 5 μm. The structure of a single bug is more obvious as the electrodeposition time increases to 15 min, and competitive growth of two or more clusters in the inset of Fig. 1(d) can be seen. With a further increase in the electrodeposition time to 30 min, these clusters evolve into larger flowers, as shown in Fig. 1(e). Furthermore, when increasing the electrodeposition time up to 45 min, all of the nanostructure assemblies develop into flowers, the heterogeneous structures with particles and flowers are formed, and the single flower has a diameter of about 15 μm (see Fig. 1(f)), and the upper flower about 5 μm, which is similar to Fig. 1(b).

In order to further clarify the formation mechanism of the superhydrophobicity, as an example, Fig. 2 shows a schematic illustration of the superhydrophobicity surface growth process. The first step is to create nucleation sites *via* process reaction growth as shown in Fig. 2(a). Oriented nanocrystals grow from these nucleation sites (Fig. 2(b)), and in the subsequent process steps, new crystals nucleate and grow on the crystals produced in previous stages. In a word, with the electrodeposition time evolution, the structure of the cathodic copper surface transforms from the turfgrass structures, loose flower structures, larger and dense flower structures, secondary flower structures, and then into tertiary or more flower structures (see Fig. 2(c)–(f)).

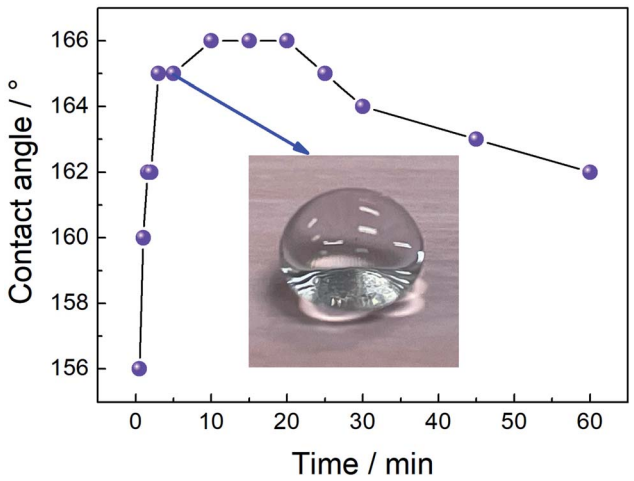

Fig. 3 The variation curve of the contact angle with the electrodeposition time.

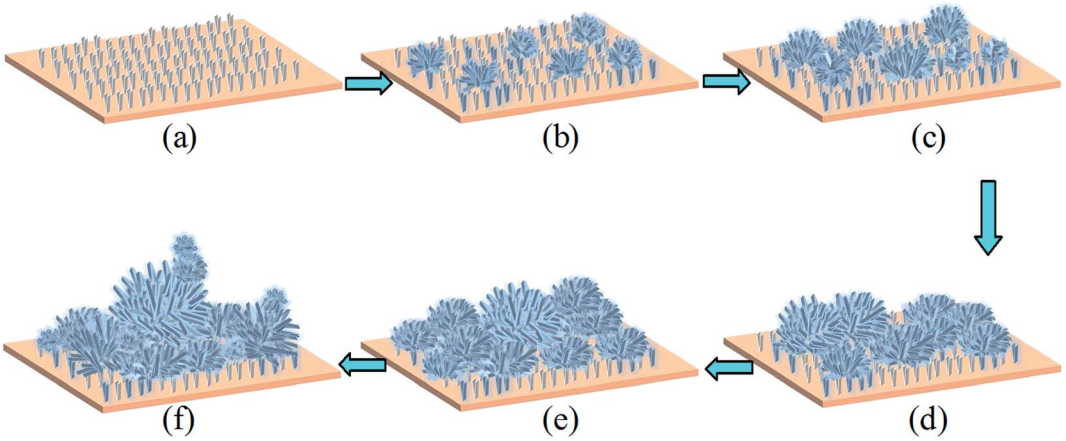

Fig. 2 Schematic illustration of the superhydrophobicity surface growth process. (a) Creation of nucleation centers similar to the turfgrass on a substrate; (b) growth of small and loose flowers on the substrate; (c) growth of big and dense flowers on small and loose flowers; (d) Ostwald growth of the big and dense flowers on the substrate, typically competition growth and merge growth; (e) secondary flower growth from the Ostwald growth patterns; (f) tertiary or more growth from the flower growth morphology.

To understand the influence of electrodeposition time on the wetting properties of the prepared Ca cathodic surfaces, the variation curve of the contact angle with the electrodeposition time is displayed in Fig. 3. As shown, the contact angle value reaches 156° at a short deposition time (0.5 min), indicating that the surface wettability has already achieved the superhydrophobic state, and strongly demonstrating that this method is quite time saving and highly efficient.[3,27] With the increase of deposition time, contact angles of surfaces show an increasing trend. When the deposition time is about 1 min, the contact angle increases to 160°. When prolonging the electrodeposition time to 3 min, the contact angle is improved to 165°. As the deposition time is further increased from 10 min to 20 min, the contact angle remains at a maximum value of 166°, and the rolling angle is less than 3°. However, further increasing the deposition time to 25 min, the contact angle decreased slightly to 165°, and then the contact angle began to decrease slowly with the electrodeposition time, but still retained good superhydrophobicity.[16]

Apart from the analyses of surface chemical compositions, according to the Cassie–Baxter equation,[28,29] the influence of surface structure on the fabrication mechanism of the superhydrophobic property is also discussed below.

$$\cos\theta_r = f\cos\theta - (1-f) \quad (1)$$

where f is the normalized interfacial area of the solid surface in contact with the liquid droplet, $(1-f)$ is that of trapped air among the micro/nano structures, r is the contact angle of micro/nano structure surfaces, and θ is that of the smooth surface. For this research, the contact angle of the smooth surface after modification with myristic acid is only about 109°, while the maximum contact angle value of the electrodeposition surface is about 166°. When these angles are substituted into eqn (1), f and $(1-f)$ can be calculated to be 0.04 and 0.96, respectively. It can be deduced that the air stored in the micro/nano structure surface prevents a water drop from infiltrating the surface, and it plays an important role in improving the wettability. Therefore, the surface exhibits superhydrophobicity within an electrodeposition time of 0.5 min; this technique has the advantages of quickness and simplicity.

The chemical compositions of the as-prepared surface were studied by XRD, FTIR and schematic diagram of the reaction progress. In Fig. 4(a), the typical XRD spectrum for the sample is displayed. As shown, in the small-angle region a set of well-defined diffraction peaks is observed. These diffraction peaks belong to the (l00) reflections, indicating that the as-prepared cathodic superhydrophobic surfaces are crystallized and regularly ordered layered structures.[30–33]

FTIR analysis was further used to investigate the absorption feature characteristic of the chemical groups of the products in the range of 4000–500 cm^{-1} as reported in Fig. 4(b). In the low-

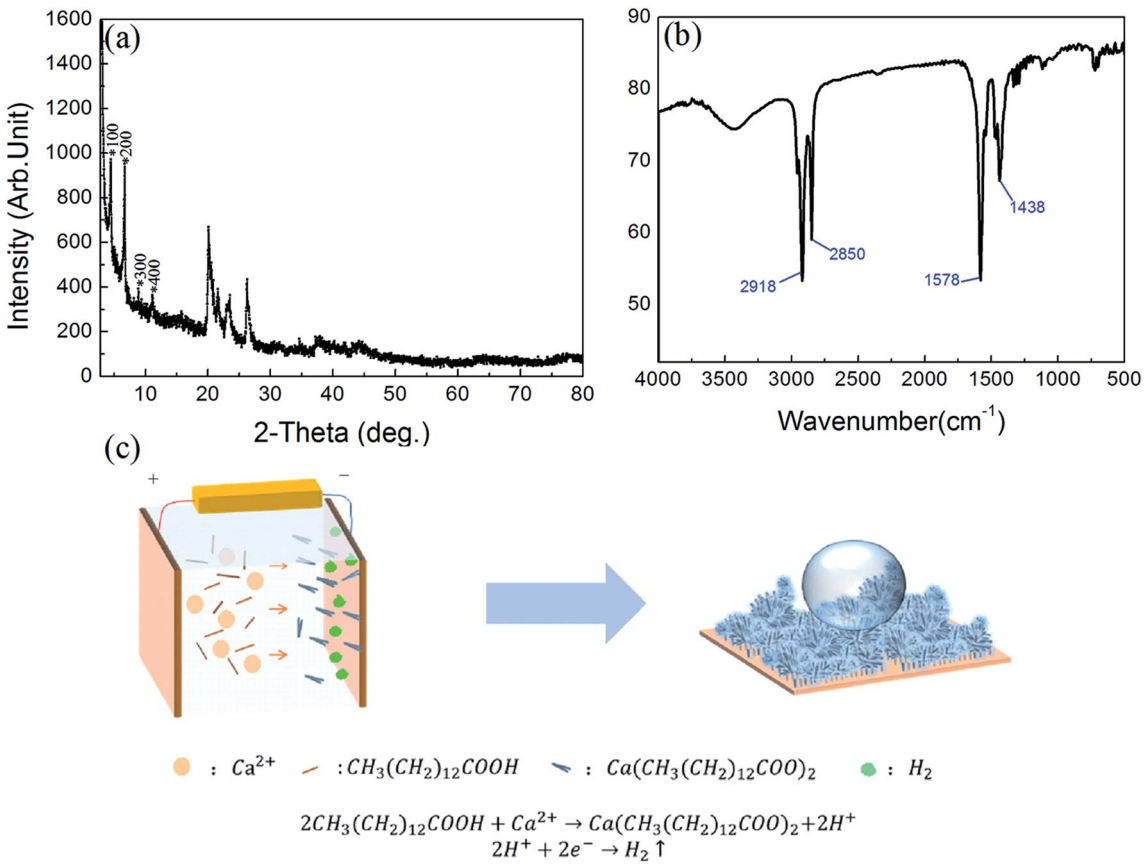

Fig. 4 (a) The corresponding XRD spectrum; (b) FTIR spectrum of the superhydrophobic surface obtained from the as-fabricated cathodic copper; (c) the schematic diagram in this experiment.

frequency region, the two strong peaks at 1438 and 1578 cm^{-1} can be assigned, respectively, to the symmetric ($\nu_s(COO^-)$) and antisymmetric ($\nu_{as}(COO^-)$) stretching vibrations of the carboxylate group. No typical peak attributable to $\nu(C{=}O)$ is identified at about 1701 cm^{-1}, indicating that the obtained sample is not contaminated with myristic acid,[27] but only its metal salt. When the frequency was higher, in the high-frequency region, the absorption peaks at 2850 cm^{-1} and 2918 cm^{-1} correspond to symmetric and asymmetric stretching vibrations of methyl groups (C–H), respectively.[34–37] As a consequence, it demonstrated that myristic acid was grafted on the surface through chemical bonding during the formation process, and calcium myristate ($Ca[CH_3(CH_2)_{12}COO]_2$) with low surface energy was formed on the cathodic copper surface, which contributed to the superhydrophobicity.

In order to clarify the electrodeposition process in this experiment, the schematic diagram in the experiment is illustrated in Fig. 4(c). The electrodeposition reaction process is explained that when the copper electrodes are immersed in the electrolyte solution with the application of DC voltage, some Ca^{2+} ions near the cathode react with myristate ($RCOO^-$) ions, and the reaction is shifted towards the formation of a carboxylate complex on the cathodic surface. In the meantime, most hydrogen (H^+) ions are ionized from the myristic acid electrolyte and generate H_2 bubbles. These released H_2 bubbles can be considered a soft template and lead to the loose micro/nano structures on the obtained superhydrophobic surface.[15,16,38] Thus, we can infer that H_2 bubbles, electrodeposited micro/nano structures, and calcium myristate with low surface energy play an important role in the transition progress. The reaction equations can be described as follows:

$$Ca^{2+} + 2CH_3(CH_2)_{12}COOH \rightarrow Ca[CH_3(CH_2)_{12}COO]_2 + 2H^+ \quad (2)$$

$$2H^+ + 2e^- \rightarrow H_2\uparrow \quad (3)$$

3.2 Effects of various experimental parameters on structures and wettability

To study the effects of preparing conditions on the electrodeposited micro/nano structures, only the concentration of calcium chloride was changed, and the others were fixed. As shown in Fig. 5(a), with increasing the concentration of calcium chloride, the value of the contact angle can reach above 160°. When increasing the concentration to 0.2 M calcium chloride, it can obtain 165°, whereas with the concentration of the calcium chloride, the value of the contact angle will decrease slowly. The reason can be deduced that the surface will become much thicker in the higher concentration of calcium chloride. It also can be seen from the inserted SEM figures that it has many clusters with about 20–30 μm diameters, which is advantageous to store many breaths of air and keep the high superhydrophobicity. Inversely, the much thicker surfaces decrease their contact angle.

The morphology and wettability of the surface at varying voltage (5, 15, 30, 45, and 60 V) are shown in Fig. 5(b). It shows the relation curve of contact angle and voltage value in 0.2 M calcium chloride and 0.1 M myristic acid solution for 5 min. When the voltage is low (5 V), the contact angle of this surface is about 153°. There are many microstructures similar to turfgrass and without flower-like structures. Upon increasing the voltage to 15 V, the contact angle increases to 158°, and its microstructures are still the turfgrass structures. Several loose flower-like structures begin to appear above the turfgrass structures. With a further increase in voltage value to 30 V, some flowers can be seen obviously in the inserted figure, and the corresponding contact angle is enlarged to 165°. It can be explained that the voltage represents the driving force of the reaction.[39] At a low voltage, the amount of hydrogen bubbles was not enough to produce a significant stir of the solution layer near the cathodic surface. Thus, the surface was primarily controlled by diffusion rather than kinetics growth; an increased voltage predominantly can dramatically increase the H_2 bubbles and reaction rate. Thus, a higher voltage has bigger and denser flower-like structures, which induce the increase of the superhydrophobicity. However, when the voltage increases to 45 V, the corresponding contact angle is decreased to 163°. When the voltage is close to 60 V, the corresponding contact angle is decreased to 159°. The reason can be that with increasing the voltage, at first electrodeposition current is 2.8×10^2 A m^{-2} at 45 V, and increases to 4.3×10^2 A m^{-2} at 60 V, which dramatically increases the nucleation rate at the cathodic surface, the clusters become larger and more compact, and result in the surface becoming over thick, and the contact angle decreases naturally.

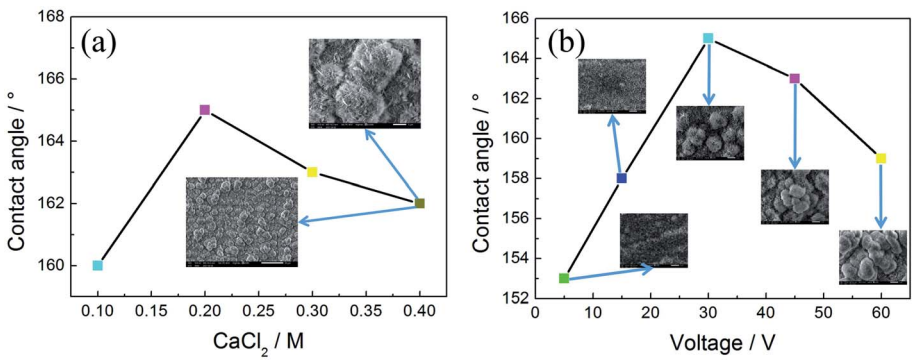

Fig. 5 (a) The curve between the content of calcium chloride and value of the contact angle; (b) the curve between the value of voltage and value of the contact angle.

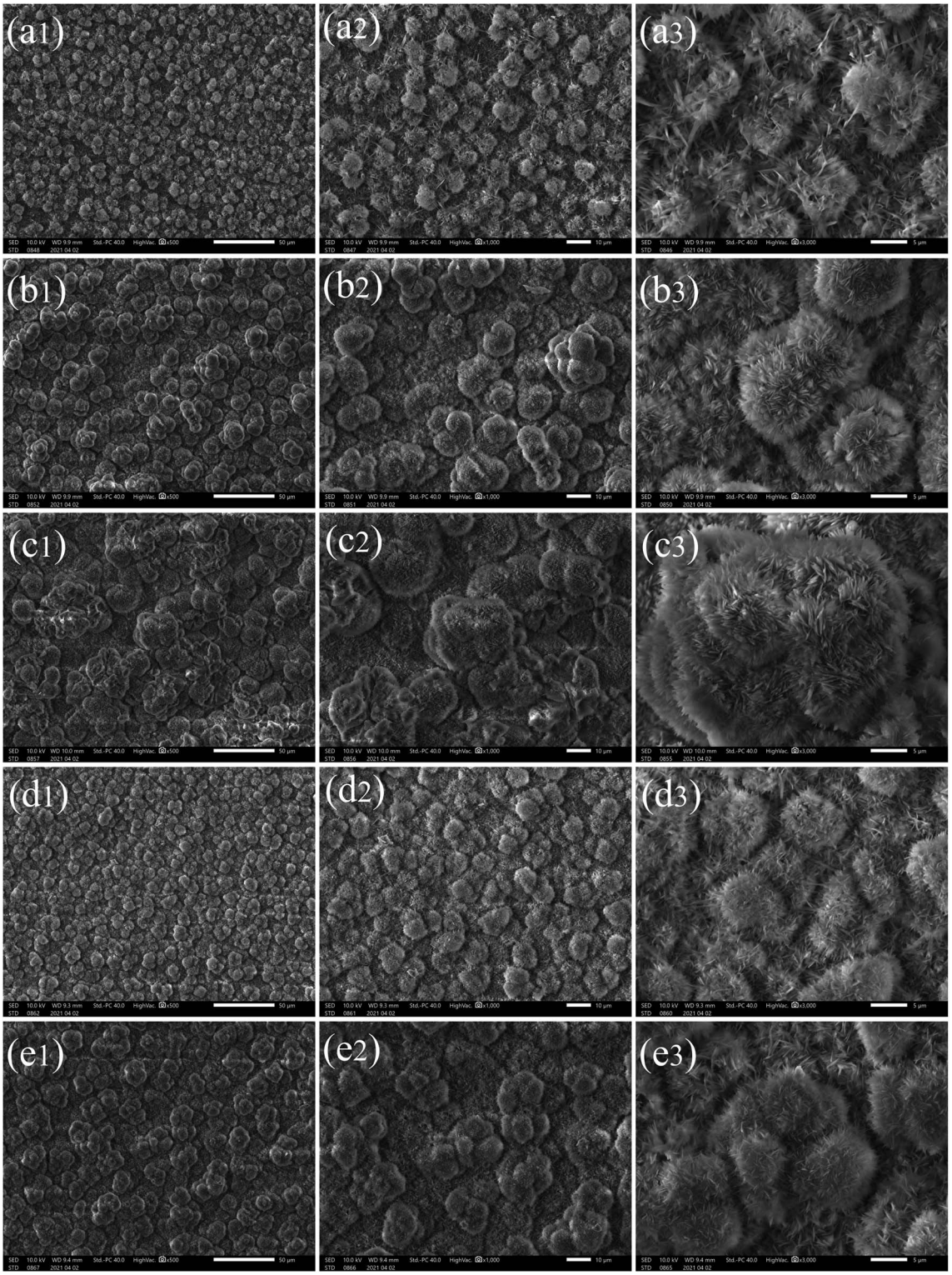

Fig. 6 SEM images of the cathodic surface in 0.2 M calcium chloride and 0.1 M myristic acid solution with a DC voltage of 30 V for different times and substrates. (a1) Low magnification 500× for stainless steel at $t = 2$ min 20 s; (a2) middle magnification 1000× for stainless steel at $t = 2$ min 20 s; (a3) high magnification 3000× for stainless steel at $t = 2$ min 20 s; (b1)–(b3) 500×, 1000×, 3000× for stainless steel at $t = 10$ min, respectively; (c1)–(c3) 500×, 1000×, 3000× for stainless steel at $t = 30$ min, respectively; (d1)–(d3) 500×, 1000×, 3000× for aluminum at $t =$ 3 min 40 s, respectively; (e1)–(e3) 500×, 1000×, 3000× for aluminum at $t = 10$ min, respectively.

In addition, to further confirm the method with universal application for conductor materials, in this section, the prepared superhydrophobic surface can be extended to other general conductor materials.

SEM images of the cathodic surface in 0.2 M calcium chloride and 0.1 M myristic acid solution with a DC voltage of 30 V for a different time on the different substrates are presented in Fig. 6. Fig. 6(a1) is the stainless steel substrate surface at a low current density of 2.4×10^2 A m^{-2} at 2 min 20 s. There appear many uniform flower-like structures on the surface. The high magnification SEM images in Fig. 6(a2) and (a3) show that the flower-like structure is composed of many compact turfgrass structures, and the diameter of each flower is about 5 μm. When the electrodeposition time is 10 min, it can be seen from Fig. 6(b1)–(b3) that the surface of stainless steel shows many compact flower-like structures similar to that of Fig. 6(a1)–(a3). Two single flower-like structures with competitive growth forming structures with a size of about 10 μm can be seen in Fig. 6(b3). When the electrodeposition time is extended to 30 min, a more compact flower structure can be seen in Fig. 6(c1) and (c2). Furthermore, it is clear from the magnification image in Fig. 6(c3) that the flower-like structures show competitive growth forming tertiary or more flower structures with a size of about 15 μm, similar to those on the copper cathodic surface in Fig. 1(f).

In addition, a pair of aluminum and stainless steel substrates are replaced under the same electrolyte conditions and can be seen in Fig. 6(d1)–(d3) and (e1)–(e3), respectively. When the electrodeposition time is 3 min 40 s, many uniform clusters appear on the substrate surface in Fig. 6(d1), and a 1000 times magnified figure in Fig. 6(d2) shows a competitive growth forming structures with a size of about 10 μm. In Fig. 6(d3), the flowers are very similar to those in Fig. 6(a3). When the electrodeposition time is prolonged to 10 min, compact clusters are shown on the substrate surface (see Fig. 6(e1)), and a 1000 times magnified figure in Fig. 6(e2) shows competitive growth of three or four flowers forming structures with a size of about 15 μm. Fig. 6(e3) shows tertiary or more flower structures.

By comparing stainless steel with aluminum and copper for an electrodeposition time of 10 min, these flowers on three kinds of substrates are very similar, and one cluster structure size of the stainless steel surface is the largest. This is mainly because the conductivity and the current density of stainless steel are the highest.

3.3 Impacting behavior of water droplets on the superhydrophobic surface

Then, to further explain the superiority of the as-prepared surface, we used a high-speed camera to study the bounce

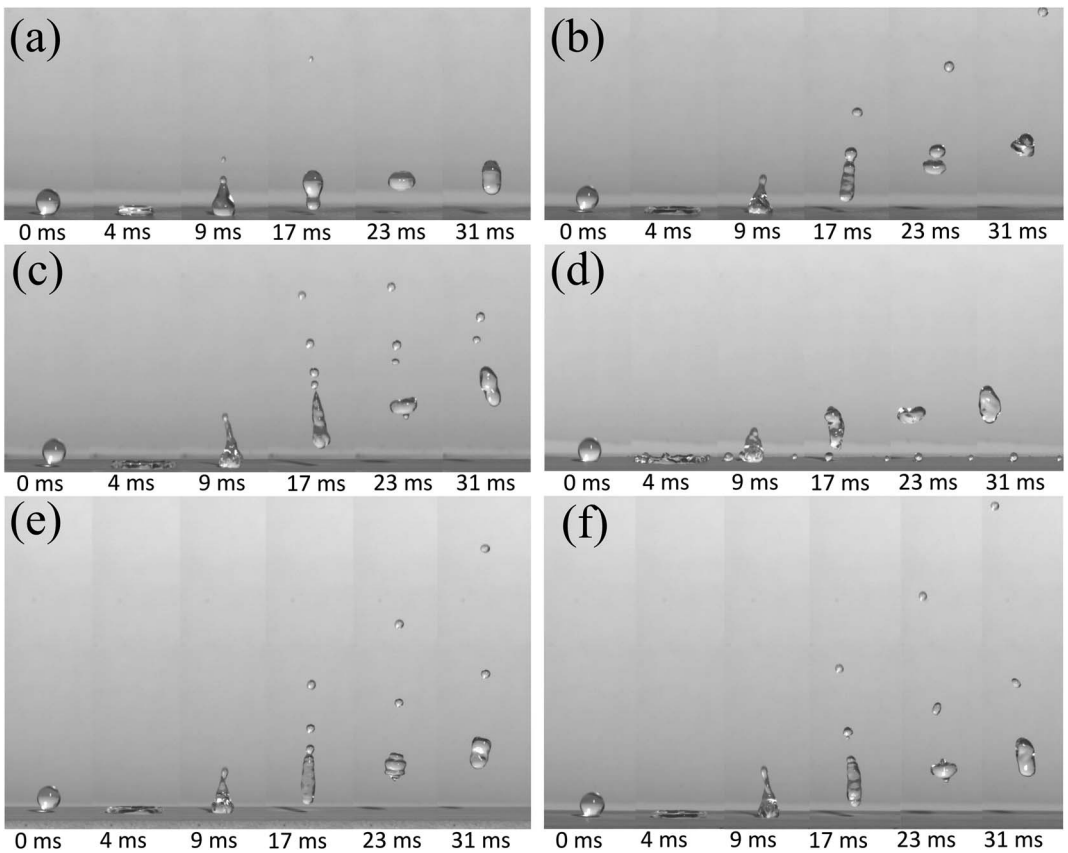

Fig. 7 The evolution process of the droplet bounce shape of the calcium superhydrophobic surface prepared by the electrodeposition of copper, aluminum, and stainless steel for 1 min. (a) $V = 0.626$ m s^{-1} for the copper substrate; (b) $V = 1.25$ m s^{-1} for the copper substrate; (c) $V = 1.53$ m s^{-1} for the copper substrate; (d) $V = 1.77$ m s^{-1} for the copper substrate; (e) $V = 1.25$ m s^{-1} for the aluminum substrate; (f) $V = 1.25$ m s^{-1} for the stainless steel substrate.

performance of water droplets impacting onto superhydrophobic surfaces. In the following experiment, 1 ml water in a syringe was divided by some number of droplets, and the average volume of every droplet is about 10 μl.

When a droplet impacts the superhydrophobic surface, it deforms and stores the kinetic energy, making the droplet recoil later on.[40–44] Fig. 7 shows the evolution process of the droplet bounce shape on the calcium superhydrophobic surface prepared by the electrodeposition of copper, aluminum, and stainless steel for 1 min, respectively. During the bounce process, the inertia forces of the droplet cause it to spread out, and during the spreading the kinetic energy of the droplet is converted into surface energy, which will be used for the retraction and rebound of the droplet. Fig. 7(a)–(d) are the bounce shapes of droplets at different velocities under a copper substrate. For a 10 μl droplet in Fig. 7(a), at 0 ms, the small droplet indicated is produced by the pinch off when the droplet separates from the syringe needle, and a similar droplet can also be observed in Fig. 7(b)–(f). A series of images of the droplet at $V = 0.626$ m s^{-1} are shown in Fig. 7(a). It can be seen from the figure that the droplet deformed, a cavity at the center of the droplet was formed, a droplet with an overlapping pancake shape was formed in the spreading stage at 4 ms, some air in the pancakes can be entrapped as the droplet retracts, and most of the air can be squeezed out when it recoiled. However, a small part of the air was trapped at the top of the cavity retracted faster than the bottom. As the retraction continued, an ejection of satellite drops was observed at 9 ms. When $t = 17$ ms, the droplets pull up again to form an approximately circular droplet. At 31 ms, it deforms again in the air. This phenomenon becomes more obvious as the velocity increases. Fig. 7(b) shows the snapshots of the impacting droplet on the superhydrophobic surface at $V = 1.25$ m s^{-1}. It was found that a pinning-like state was observed when $t = 9$ ms and the droplets were greatly elongated before taking off. This phenomenon is more clear when $V = 1.53$ m s^{-1} in Fig. 7(c); as shown, the main droplet and four satellite drops rebound taking off the surface at 17 ms.

When the velocity reaches $V = 1.77$ m s^{-1}, as shown in Fig. 7(d), the droplets were torn into a large droplet and two satellite drops at 9 ms. The reason is maybe the larger pinning force and rebound velocity. The main part of the droplet rebounded off again, while the satellite drops were pinned on the surface with Wenzel state at 17 ms. Nevertheless, when the main droplet impacted the surface again, moreover, it was also observed that the bouncing height of the main droplets was not as superior as that of droplets at low velocities. This rule is similar to the results reported in the related literature;[45] that is, the greater the initial velocity, the stronger the bounce performance of the droplet, but the best bounce performance within a certain range.

Next, the versatility of the bounce performance was further verified under the aluminum and stainless steel substrates under the same preparation condition with a copper substrate. As shown in Fig. 7(e) and (f), at 17 ms, two satellite drops can be seen on the aluminum substrate and stainless steel, which means that when the droplets impacted the surface of the substrate, the rebound velocity was greater. These results proved that the metal substrate plays an effective role in promoting the bounce of the droplets.

Although many methods and technologies to fabricate superhydrophobic surfaces have been reported, few products have been launched using such surfaces. This is mainly because these surfaces are generally very weak to resist mechanical contact.[46] In real environmental conditions, the destruction of surface structures by external forces can lead to a very fast loss of superhydrophobicity. Thus, we investigated the changes of these samples by SEM structures and bounce performance under a manual pressing force of a thumb by a glass slide. Before the pressing force, when the electrodeposition time was prolonged to 5 min for the copper substrate, it can be seen from the SEM image magnified 1000 times in Fig. 8(a) that some large flower-like structures grow on the surface of the substrate before pressing. Similar to Fig. 7, at 0 ms, the small droplet indicated is produced as in Fig. 7. As shown, the impact velocity of $V = 1.25$ m s^{-1} on the surface droplets shows that, at 17 ms, a jet is gradually developed, and cut off and a satellite drop is separated. After a short time, the jet leaves the surface. When $t = 23$ ms, there are two different heights for the drops, and at $t = 31$ ms, they coalesced into a large droplet with each other, and rebounded off again.

After the superhydrophobicity surface was pressed by the pressing force of the thumb, about 98 N, the corresponding SEM image is shown in Fig. 8(b). It can be seen that the main part of the displayed flower has formed black, dense structures *via* applying a pressing force. Under the same size droplet impact and the same velocity $V = 1.25$ m s^{-1}, the phenomenon of a jet breakup is no longer the same as that described in Fig. 8(a). At $t = 17$ ms, after the separation of the first satellite drop, separation into the second satellite drop has already begun. At $t = 23$ ms, the large, medium and small drops are clearly distributed at different bounce heights, respectively. At $t = 31$ ms, the distance between the small droplet and the main droplet is further increased. Thus, we can conclude that the superhydrophobic surface prepared by this method is a soft surface. After being pressed by a pressing force, its hardness increases, but the superhydrophobic performance is not weakened. Inversely, the bouncing performance is enhanced.

When magnifying the surface microstructures 3000 times, in Fig. 8(c), the SEM shows that the structure of each flower is about 5 μm. If the impact velocity increases to 1.53 m s^{-1}, at 17 ms, it is obvious that with the increase of impact velocity, the number of satellite drops increases. When $t = 23$ ms, three drops of different sizes and heights are clearly visible. At 68 ms, it can be seen that the rebound height is much higher than that of Fig. 8(a), which shows that the velocity obviously affects the rebound height of the droplet. On the contrary, under the condition of keeping the water droplet velocity, the impact progress was carried out on the same substrate which is pressed by the pressing force strength, and it was found that its bounce performance was further enhanced in Fig. 8(d). It can be clearly seen that at 17 ms, three satellite drops are formed, and separation into the fourth satellite drop has already begun. From the beginning, when $t = 23$ ms, four droplets are formed, and when

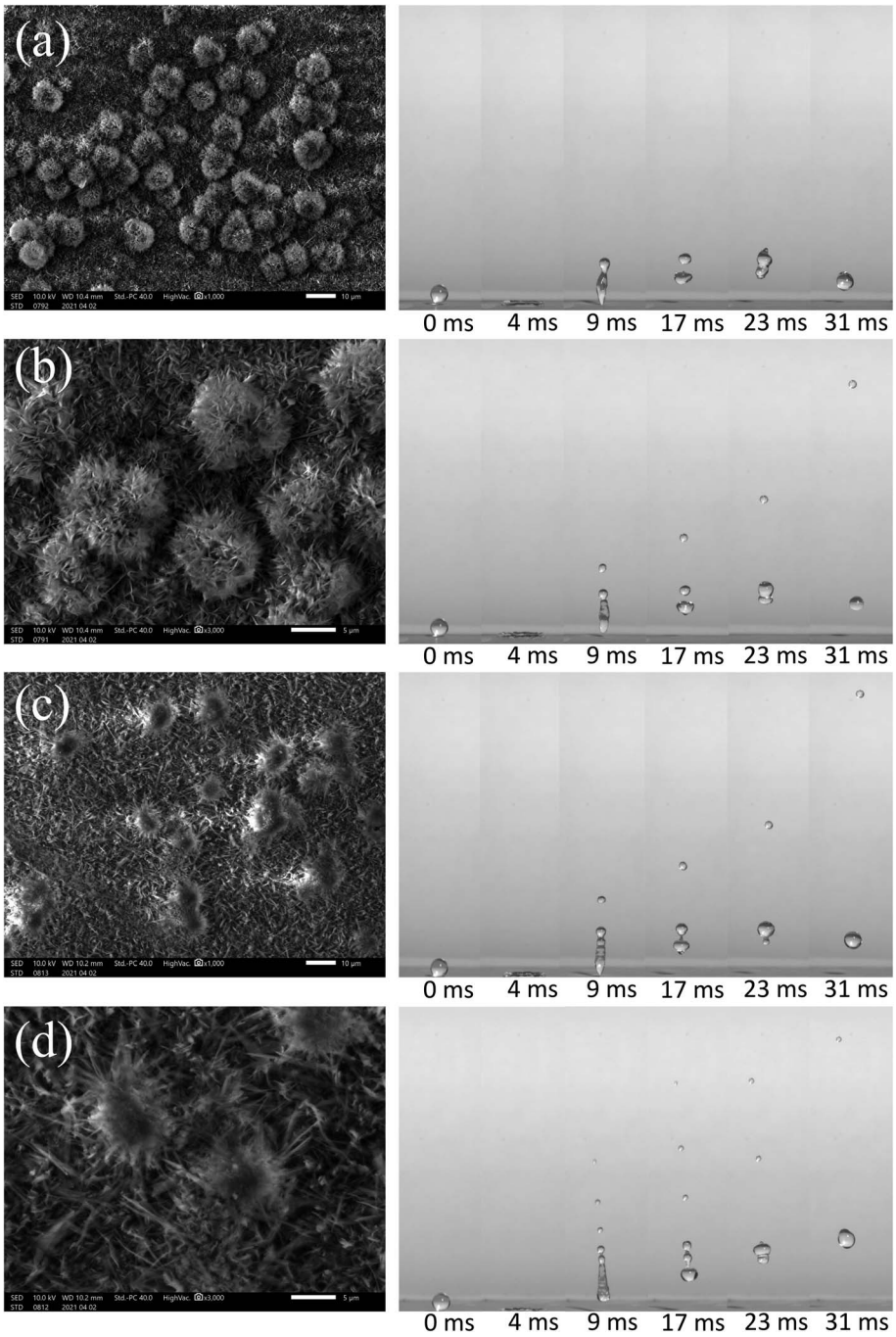

Fig. 8 The SEM structure and impact performance of the surface before and after the pressing force of a thumb for 5 min on the electrodeposited copper surface. (a) 1000× SEM for the copper substrate at 5 min, $V = 1.25$ m s^{-1}; (b) 3000× SEM for the copper substrate at 5 min, $V = 1.53$ m s^{-1}; (c) 1000× SEM for the same copper substrate with the pressing force at 5 min, $V = 1.25$ m s^{-1}; (d) 3000× SEM for the same copper substrate with the pressing force at 5 min, $V = 1.53$ m s^{-1}.

$t = 68$ ms, the rebound height becomes higher. The reason can be that the droplet has larger potential energy which makes the droplet have greater kinetic energy during the impact process. Therefore, the rebound velocity increases with the increase of the droplet bounding velocity. The larger the rebound velocity the smaller the radius of the jet column, the thinner the column is, and the easier it is to be cut off. Therefore, the number of satellite drops increases with the bounding velocity and manual pressing progress.

Fig. 9 shows a comparison diagram of droplet rebound characteristics of superhydrophobic surfaces prepared on different substrates before and after a pressing force by a glass slide. Fig. 9(a) reveals the bouncing result of a copper substrate for 30 min electrodeposition at $V = 1.25$ m s^{-1}. It should be noted that 0 ms is also set as the time that the droplet just

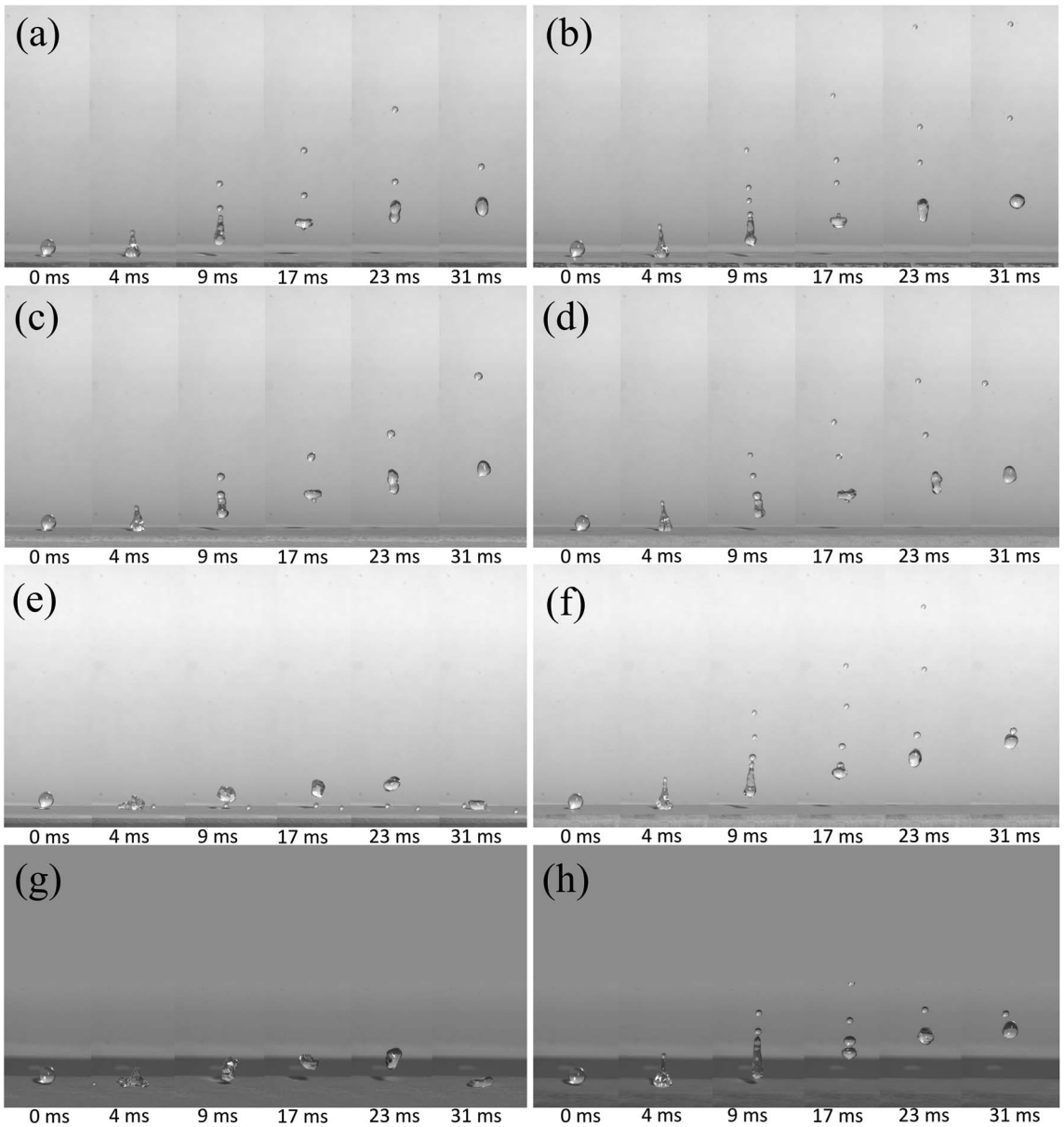

Fig. 9 The impact performance of the surface before and after the pressing force of the thumb for different substrates. (a) $V = 1.25$ m s^{-1} for the copper substrate at 30 min; (b) $V = 1.25$ m s^{-1} for the copper substrate with the pressing force at 30 min; (c) $V = 1.25$ m s^{-1} for the aluminum substrate at $t = 30$ min; (d) $V = 1.25$ m s^{-1} for the aluminum substrate with the pressing force at 30 min; (e) $V = 1.53$ m s^{-1} for the aluminum substrate at 15 min; (f) $V = 1.53$ m s^{-1} for the aluminum substrate with the pressing force at 15 min; (g) $V = 1.53$ m s^{-1} for the stainless steel substrate at 15 min, overlook views with a tilt angle of about 5°; (h) $V = 1.53$ m s^{-1} for the stainless steel substrate with the pressing force at 15 min, overlook views with a tilt angle of about 5°.

contacts the superhydrophobic surface. At 9 ms, it forms a jet shape, and the formed jet gradually elongates and thins rather than rapidly breaking up. At a time of 17 ms, droplets just now pinch off the surface, and two satellite drops are successively developed on the tip of the jet. By comparing it with superhydrophobic copper surfaces (Fig. 7(b) and 8(a)), it can be observed that the rebound performance of the superhydrophobic surface with an electrodeposition time of 30 min is better than that of the latter. And three satellite drops can be observed appearing at 17 ms after pressing the surface (Fig. 9(b)), and we found that the satellite drops fall back to the surface, coalesce with main droplets, and then completely rebound. It proved that rebound performance is better after the pressing force.

Fig. 9(c) and (d) show the rebound behavior of the water droplets on the aluminum surface for 30 min electrodeposition at $V = 1.25$ m s^{-1}, respectively. It can be seen that, at 68 ms, the superhydrophobic surface after the pressing force has a higher rebound height. Fig. 9(e) and (f) show the rebound behavior of water droplets with $V = 1.53$ m s^{-1} impacting the aluminum superhydrophobic surface for 15 min electrodeposition. Before pressing, an impacting droplet is deformed during spreading

and forms an oval shape. When the maximum extension is reached (9 ms–17 ms), then it resumes back to the spherical shape, and takes off with a jet and small satellite drops similar to that of Fig. 9(a)–(d). The reason maybe is that the aluminum surface has grown a thicker surface than that of 1 minute, and the prepared surface is a soft surface, so the droplets will collide and bounce at a certain speed. It consumes a part of the momentum, so that its bounce height is lower and the chance of satellite drop formation is greatly reduced. After pressing, as shown in Fig. 9(f), the droplet bounces up obviously, and the phenomenon is similar to that of Fig. 9(a)–(e). It is also proved that the pressing force can improve the soft surface superhydrophobicity.

In order to further study the rebound behavior, we imaged the rebound behavior of water droplets on the stainless steel superhydrophobic surface with a tilt angle of about 5°. Fig. 9(g) shows the water droplet rebound behavior of stainless steel for 15 min electrodeposition at $V = 1.53$ m s^{-1}. It can be seen more clearly that it impacts the surface to form a round cake shape at 4 ms. In the retraction progress, at 10 ms, one satellite drop cannot follow the main droplet's receding motion and thus pinches off on the surface (9–68 ms in Fig. 9(g)). However, the main droplet bounces at $t = 10$ ms, and then leaves the small satellite drop pinning on the surface. Fortunately, after the pressing force, the surface can obtain a bounce ability similar to that in Fig. 9(c).

Therefore, we can conclude that within a certain range of droplet impact velocity, the larger the velocity, the stronger the bounce performance. At the same impact velocity, the rebound performance of aluminum and stainless steel is better than that of the copper substrate. The main reason is that the hardness of aluminum and stainless steel is higher than that of stainless steel. The proper increase of the electrodeposition time is advantageous to the rebound performance at the same velocity and the same substrate. More importantly, the superhydrophobic surface that is pressed with a glass slide by the pressing force of the thumb can significantly strengthen the rebound performance of water droplets. The reason is believed to be mainly due to the fact that the flower-like structures on the surface become denser, harder, and consume less energy for the bounce of droplets after the pressing force.

4. Conclusions

In conclusion, we have successfully reported a simple one-step electrodeposition process to construct a soft calcium superhydrophobic surface on the cathodic substrate with an electrolyte solution, and its rebound performance was also studied systematically. The needed shortest electrodeposition time can be largely shortened to 0.5 min. A maximum contact angle of 166° and a low rolling angle of less than 3° are achieved on the prepared cathodic copper surface. The cooperation of H_2 bubbles, flower-like structures, and calcium myristate with low surface energy play an important role in adjusting surface wettability. Such unique surface structures can contribute to trapping a large amount of air and showing a superhydrophobic performance. Moreover, this kind of calcium superhydrophobic surface has an excellent bound performance. After the pressing force, the bound performance of the as-prepared surface will be increased. The technique is expected to provide a promising way for the large-scale fabrication of superhydrophobic surfaces and promote the bound performance by a simple pressing force.

Conflicts of interest

The authors declare that they have no known competing financial interests or personal relationships that could have appeared to influence the work reported in this paper.

Acknowledgements

This work was supported by the National Natural Science Foundation of China (no. U1806219, 52073232), the Natural Science Foundation of Shannxi Province, China (no. 2019JM-157, 2020JC-11, 2020JM-111), and National undergraduate innovation and entrepreneurship training program (no. 202110699148).

References

1 W. Zhang, D. Wang, Z. Sun, J. Song and X. Deng, *Chem. Soc. Rev.*, 2021, **50**, 4031.
2 B. Su, Y. Tian and L. Jiang, *J. Am. Chem. Soc.*, 2016, **138**(6), 1727–1748.
3 L. Hou, N. Wang, J. Wu, Z. Cui, L. Jiang and Y. Zhao, *Adv. Funct. Mater.*, 2018, **28**(49), 1801114.
4 B. Bhushan and Y. Jung, *Prog. Mater. Sci.*, 2011, **56**(1), 1–108.
5 W. Barthlott and C. Neinhuis, *Planta*, 1997, **202**(1), 1–8.
6 C. Neinhuis and W. Barthlott, *Ann. Bot.*, 1997, **79**(6), 667–677.
7 J. Li, J. Tian, Y. Gao, R. Qin, H. Pi, M. Li and P. Yang, *Chem. Eng. J.*, 2021, **410**, 128347.
8 S. Rasouli, N. Rezaei, H. Hamedi, S. Zendehboudi and X. Duan, *Mater. Des.*, 2021, **204**, 109599.
9 K. Ellinas, P. Dimitrakellis, P. Sarkiris and E. Gogolides, *Processes*, 2021, **9**(4), 666.
10 P. Roach, N. Shirtcliffe and M. Newton, *Soft Matter*, 2008, **4**(2), 224–240.
11 Y. Zhang, H. Xia, E. Kim and H. Sun, *Soft Matter*, 2012, **8**(44), 11217–11231.
12 K. Gray, B. Liba, Y. Wang, Y. Cheng, G. Rubloff, W. Bentley, A. Montembault, I. Royaud, L. David and G. Payne, *Biomacromolecules*, 2012, **13**(4), 1181–1189.
13 J. Tam, G. Palumbo and U. Erb, *Materials*, 2016, **9**(3), 151.
14 Z. Chen, L. Hao, A. Chen, Q. Song and C. Chen, *Electrochim. Acta*, 2012, **59**, 168–171.
15 Z. Chen, L. Hao and C. Chen, *Colloids Surf., A*, 2012, **401**, 1–7.
16 T. Darmanin, E. Givenchy, S. Amigoni and F. Guittard, *Adv. Mater.*, 2013, **25**(10), 1378–1394.
17 L. Shen, M. Fan, M. Qiu, W. Jiang and Z. Wang, *Appl. Surf. Sci.*, 2019, **483**, 706–712.
18 C. Hu, X. Xie, H. Zheng, Y. Qing and K. Ren, *New J. Chem.*, 2020, **44**(21), 8890–8901.

19 Y. Liu, X. Yin, J. Zhang, S. Yu, Z. Han and L. Ren, *Electrochim. Acta*, 2014, **125**, 395–403.
20 W. Simka, D. Puszczyk and G. Nawrat, *Electrochim. Acta*, 2009, **54**(23), 5307–5319.
21 Y. Li, W. Jia, Y. Song and X. Xia, *Chem. Mater.*, 2007, **19**(23), 5758–5764.
22 Y. Li, Y. Song, C. Yang and X. Xia, *Electrochem. Commun.*, 2007, **9**(5), 981–988.
23 X. Yao, L. Xu and L. Jiang, *Adv. Funct. Mater.*, 2010, **20**(19), 3343–3349.
24 C. Tang, Z. Huang and H. Allen, *J. Phys. Chem. B*, 2011, **115**(1), 34–40.
25 J. Lee, K. Jung, S. Lee and J. Ko, *Appl. Surf. Sci.*, 2016, **369**, 163–169.
26 J. Kuang, Z. Ba, Z. Li, Z. Wang and Z. Qiu, *Appl. Surf. Sci.*, 2020, **501**, 144137.
27 S. Wang, L. Feng and L. Jiang, *Adv. Mater.*, 2006, **18**(6), 767–770.
28 A. Cassie and S. Baxter, *Trans. Faraday Soc.*, 1944, **40**, 546–551.
29 A. Milne and A. Amirfazli, *Adv. Colloid Interface Sci.*, 2012, **170**(1–2), 48–55.
30 M. Gönen, S. Öztürk, D. Balköse, S. Okur and S. Ülkü, *Ind. Eng. Chem. Res.*, 2010, **49**(4), 1732–1736.
31 M. Segovia, K. Lemus, M. Moreno, M. SantaAna, G. González, B. Ballesteros, C. Sotomayor and E. Benavente, *Mater. Res. Bull.*, 2011, **46**(11), 2191–2195.
32 D. Roy, N. Das and P. Gupta, *Appl. Surf. Sci.*, 2013, **271**, 394–401.
33 M. Popescu, T. Gutberlet, M. Kastowsky, P. Koch and H. Bradaczek, *Thin Solid Films*, 1997, **304**(1–2), 323–326.
34 Y. Wang, X. Du, L. Guo and H. Liu, *J. Chem. Phys.*, 2006, **124**(13), 134706.
35 S. H. Liang, T. Yu, D. P. Liu, W. X. Wang, Y. P. Wang and X. F. Han, *J. Appl. Phys.*, 2011, **109**(7), 07C115.
36 Z. Kang, J. Zhang and L. Niu, *Surf. Coat. Technol.*, 2018, **334**, 84–89.
37 S. Mukherjee and A. Datta, *Phys. Rev. E: Stat., Nonlinear, Soft Matter Phys.*, 2011, **84**(4), 041601.
38 S. Wen and J. Szpunar, *Electrochim. Acta*, 2005, **50**(12), 2393–2399.
39 B. Lim and Y. Xia, *Angew. Chem., Int. Ed.*, 2011, **50**(1), 76–85.
40 L. Chen, Z. Xiao, P. Chan, Y. Lee and Z. Li, *Appl. Surf. Sci.*, 2011, **257**(21), 8857–8863.
41 L. Chen, Y. Wang, X. Peng, Q. Zhu and K. Zhang, *Macromolecules*, 2018, **51**(19), 7817–7827.
42 C. Lv, P. Hao, X. Zhang and F. He, *Appl. Phys. Lett.*, 2016, **108**(14), 141602.
43 S. Pan, R. Guo, M. Björnmalm, J. Richardson, L. Li, C. Peng, N. Bertleff-Zieschang, W. Xu, J. Jiang and F. Caruso, *Nat. Mater.*, 2018, **17**(11), 1040–1047.
44 M. Muschi, B. Brudieu, J. Teisseire and A. Sauret, *Soft Matter*, 2018, **14**(7), 1100–1107.
45 M. Chubynsky, K. Belousov, D. Lockerby and J. Sprittles, *Phys. Rev. Lett.*, 2020, **124**, 084501.
46 D. Wang, Q. Sun, M. Hokkanen, C. Zhang, F. Lin, Q. Liu, S. Zhu, T. Zhou, Q. Chang, B. He, Q. Zhou, L. Chen, Z. Wang, R. Ras and X. Deng, *Nature*, 2020, **582**(7810), 55–59.